Concentration-Dependent Photon-Echo Decay in Ruby*†

A. Compaan‡§
Department of Physics, The University of Chicago, Chicago, Illinois 60637
(Received 30 August 1971)

A detailed experimental study is reported of the decay of circularly polarized photon echoes as a function of Cr concentration in samples ranging from 0.006 to 1.2 wt.% Cr_2O_3 in Al_2O_3. The decay is found to be independent of temperature in the liquid-helium range and generally depends on the pulse separation τ as $\exp(-K\tau^{1/2})$ with the decay constant K proportional to the square root of the Cr concentration. The measured decay is independent of external magnetic field in the range 1.5–6 kG except at 1.06 kG, where modified decays are observed. A theoretical analysis is made of photon-echo decay in terms of spin flips of echo ions resulting from Cr-Cr magnetic interactions and yields good agreement with the observed decays. Spectral diffusion, modified for photon echoes, is shown not to be an important effect. However, anomalously slow decay is observed in some samples when the laser is tuned to the long-wavelength tail of the sample absorption line and the spectral-diffusion mechanism may apply here. The photon-echo-decay measurements are compared with spin-resonance and available spin-echo data in ruby. Also, it is inferred that resonant optical energy transfer is not an important photon-echo-decay mechanism even in the darkest sample studied.

I. INTRODUCTION

The photon-echo effect[1] has been demonstrated to be a useful technique for obtaining information on relaxation processes in crystals[2] and gases.[3] Photon-echo measurement of a phonon-assisted excited-state relaxation in ruby has been accomplished by an indirect temperature-variation method,[2] and collisional relaxation rates in a gas have been measured by a direct echo-intensity–vs–pulse-separation technique performed with two gas lasers pulsed sequentially.[3] However, this two-laser technique for direct echo-decay measurements is precluded in the case of ruby lasers and for many other lasers principally as a result of temperature-dependent shifts of the lasing frequency.[4,5] We report here on the use of a single Q-switched ruby laser in combination with a variable optical delay line in a detailed study of photon-echo decay in ruby. The observed decays are independent of temperature, in contrast with those previously measured,[2] and depend strongly on the Cr concentration in ruby.

Considerable study has been made of concentration-dependent effects in ruby such as resonant single-ion–single-ion optical energy transfer,[6] pair spectra,[7] and the possible long-range exchange interactions between Cr ions.[8] However, the influence of these effects on the optical spectra often cannot be studied (except for the nearest-neighbor pairs) because of the relatively large inhomogeneous broadening due to static crystalline-field variations.[9,10] A photon-echo investigation is ideally suited to this situation since the rephasing which produces the superradiant echo state is unaffected by the large static inhomogeneous broadening of the ruby R_1 line. The echo decay results only from effects which either remove ions from the two-level echo system or which disrupt the phase memory. Thus, the detailed shape of the echo decay as a function of time gives a direct measure of the various dynamic interactions of the Cr ion with its environment; such information may sometimes be obtained indirectly by linewidth measurement but is more often obscured entirely.

This paper is organized into five sections. In Sec. II A we shall describe the experimental apparatus and the techniques for rapidly varying the pulse separation, in Sec. II B the laser-sample resonance conditions, and in Sec. II C the results of the echo-intensity–vs–pulse-separation measurements obtained at liquid-helium temperatures from several ruby crystals of varying Cr concentration. We also present in Sec. II C data showing the presence of faster decays at the 2.06-kG ground-state level-crossing field, and other data showing a significantly slower decay when the laser is tuned toward the long-wavelength side of the sample absorption line. Section III contains an analysis of two types of concentration-dependent decay mechanisms which indicates that the observed decays may be understood very well on the basis of Cr-Cr magnetic dipolar interactions. The principal result of the analysis is the prediction of decays which are not simple exponentials but, rather, have the form $\exp(-K\tau^{1/2})$, where τ is the pulse separation and where the decay constant K is proportional to the *square root* of the Cr ion concentration. In Sec. IV we (i) interpret the anomalously slow decay observed in the long-wavelength tail of the absorption line of the 0.03 wt.% sample, (ii) analyze the faster decays observed at 2.06 kG in the $^4A_2(+\frac{1}{2})$

$\rightarrow {}^2E(\bar{E})(+\frac{1}{2})$ transition, (iii) comment on the limiting echo decay in small magnetic fields, and (iv) compare our photon-echo-decay measurements with available data from spin-resonance measurements in ruby.

We wish to emphasize at this point that we shall not discuss in this paper the effects of the Cr spin interactions with its nearest-neighbor Al nuclear spins which give rise to modulations of the photon-echo amplitude as a function of pulse separation.[11,12] This effect, which has also been observed and analyzed in several spin-echo systems,[13] is independent of Cr concentration in ruby[11] and strongly affects the photon echo when the external magnetic field B_0 is not parallel to the c axis. These Cr-Al effects are the subject of a forthcoming paper by Lambert.

Throughout this paper we shall refer to sample concentration for identification purposes as $x\%$. This abbreviated nomenclature is intended to mean weight percent (wt.%) of Cr_2O_3 in Al_2O_3, as specified by the manufacturer of the crystals. Fractional atomic concentration will be described as $x\times10^{-n}$, without reference to percent.

II. PHOTON-ECHO-DECAY MEASUREMENTS

A. Experimental Apparatus

The experimental arrangement for observing circularly polarized photon echoes is indicated schematically in Fig. 1. The liquid-nitrogen-cooled ruby laser,[1] with a Kerr-cell Q switch, produced a 15-nsec pulse of approximately 200-kW peak power. Both the direct pulse and the second pulse, from the optical delay line described below, were focused through a fused quartz window to a cross-sectional area of about 0.02 mm^2 onto the conduction-cooled 1-mm-thick ruby sample. The sample was attached by a copper cold finger to the liquid-helium bath and the temperature, monitored with a Honeywell germanium resistance thermometer, was maintained between 6 and 9 °K. The sample Dewar was mounted between the pole faces of a 6-in. Varian magnet. Thin mica quarter-wave plates were used to establish the circular polarization of the incident pulses and to convert the circularly polarized echo into plane polarization prior to detection by the photomultiplier plus Kerr cell shutter assembly. The pulses were displayed on a Tektronix 585A oscilloscope. To generate circularly polarized photon echoes, the incident pulses must propagate parallel to the c axis of the crystal ($\vec{k}\parallel\vec{c}$), and, in addition, the external magnetic field $\vec{B}_0$ must be applied parallel to the c axis. This required the use of small mirrors near the magnet pole faces with the quarter-wave plates mounted between these and the sample Dewar. The circularly polarized echoes were necessarily observed from 0° samples, c axis normal to the face of the crystal, and either transition (see Sec. II B) was selected by simply reversing the magnetic field. Additional data were taken on several 90° samples using plane-polarized pulses with $\vec{B}_0\parallel\vec{c}$ and both $\vec{k}$ and $\vec{E}\perp\vec{c}$, where $\vec{E}$ is the electric field vector of the incident light. In this case the optical arrangement at the sample Dewar was much simpler,[1] with neither quarter-wave plates nor mirrors needed and the beams passing through the Dewar parallel to the magnet pole faces. Both the 0° and 90° Verneuil ruby samples were obtained from the Adolph Meller Company with nominal concentrations ranging from 0.006 to 1.2% Cr_2O_3 in Al_2O_3.

For the experiments on the low-concentration samples (0.006, 0.03, 0.1%) the 1.5-m-confocal spherical-mirror delay line,[1] which is used to generate the second-pulse delays τ, was operated in a

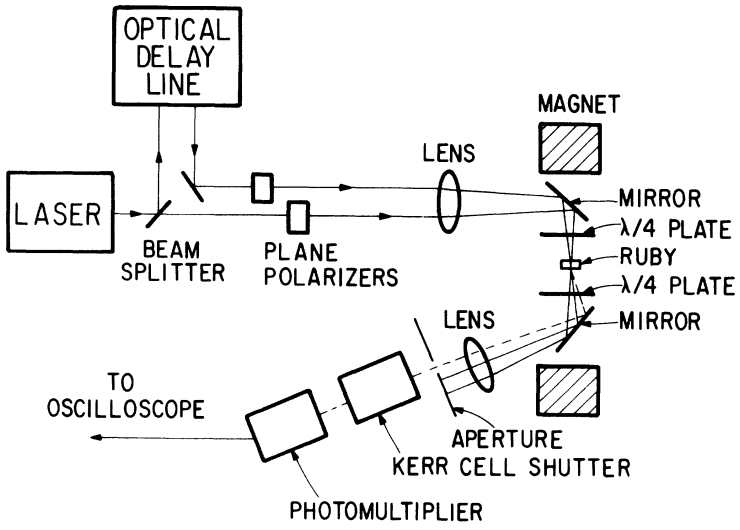

FIG. 1. Experimental arrangement for observing circularly polarized photon echoes.

reentrant mode in which the beam is reintroduced after the first exit. This made it possible to double the maximum usable pulse delay to approximately 600 nsec. Furthermore, by properly reintroducing the beam, the delay line was made to operate in a manner that automatically compensated for beam deflections resulting from vibration of the mirrors or from air currents between the mirrors. Normally these effects are approximately additive for each round trip between mirrors and become severe when more than 20 or so passes are required. The reentrant mode also greatly facilitated rapid adjustments from one pulse separation to the next during a single experimental run. The delay-line mirrors have a reflectivity of 99.9% at 6934 Å, and by direct measurement the second-pulse attenuation for a 300-nsec delay was less than 15%. Measurements of echo intensity vs second-pulse intensity showed that we were operating with average pulse "areas" $\theta \cong \pi$ in the multimode incident beams, in which case the echo intensity is relatively independent of second-pulse intensity.[14] The pulse area θ is defined as $\theta = (p/\hbar)\int \mathcal{E}\, dt$, where p is the dipole moment of the transition and $\mathcal{E}$ is the time-dependent envelope of the electric field. Using these data we estimate the echo intensity with $\tau = 580$ nsec to have diminished by less than 10% as a consequence of the loss in second-pulse intensity and therefore it is neglected in the data analysis.

Rapid adjustment of the delay-line mirrors was facilitated through the use of a collimated white-light source whose beam was accurately collinear with the ruby-laser beam. Maintaining the spatial overlap of the pulses in the sample is extremely important and was repeatedly checked during the course of a single experimental run by observing, on a piece of developed polaroid film, the two small spots burned by the beams at the focus of the first lens. Each datum point was obtained by averaging six to ten echo pulses, and in general the data were reproducible during a run to within the rms fluctuations, and the decay curves for a given sample were consistent from one run to the next.

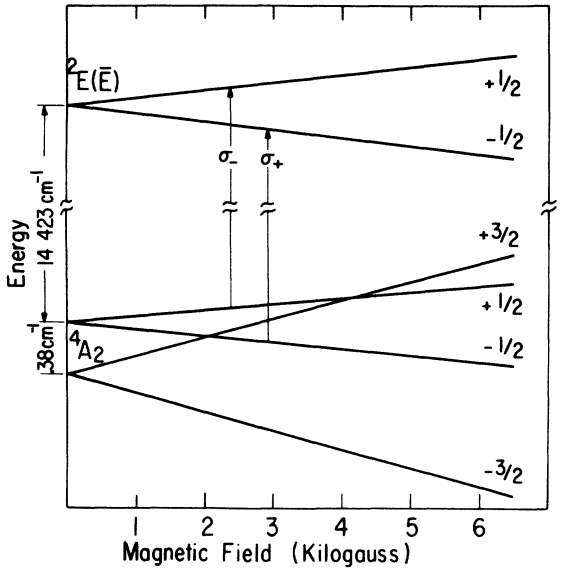

FIG. 2. Energy levels of ruby R_1 line for magnetic field applied parallel to the c axis. $\sigma-$ and $\sigma+$ denote the two independent circularly polarized transitions which were studied. The m values are labeled in accordance with Ref. 15.

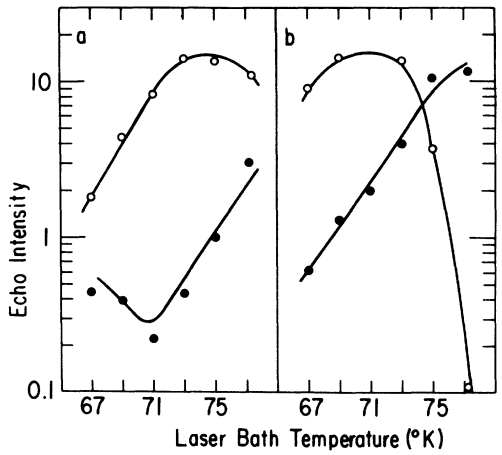

FIG. 3. Echo intensity as a function of the liquid-nitrogen-bath temperature of the laser, with a pulse separation of 60 nsec and for two different laser-pulsing conditions as described in the text. A magnetic field of 6 kG was applied parallel to the c axis of the 0.03% ruby sample. Open circles and closed circles refer to $(\frac{1}{2} \rightarrow \frac{1}{2})$ and $(-\frac{1}{2} \rightarrow -\frac{1}{2})$ transitions, respectively. The increase in the $(-\frac{1}{2} \rightarrow -\frac{1}{2})$ echo intensity at low temperatures in (a) arises from weak laser emission to the $^4A(\pm\frac{1}{2})$ ground state.

B. Laser—Sample Resonance Conditions

In this experiment we studied photon echoes from two of the four circularly polarized $^4A_2(m) \rightarrow {}^2E(\bar{E})(m')$ transitions in ruby[15] (see Fig. 2). These two transitions $(m = +\frac{1}{2} \rightarrow m' = +\frac{1}{2})$ and $(m = -\frac{1}{2} \rightarrow m' = -\frac{1}{2})$ exhibit only a slight magnetic field tuning or Zeeman shift due to the difference in g factors between ground $(g = 1.98)$ and excited states $(g' = 2.44)$, where the primed quantities refer to the optical excited state. Thus, echoes could be observed at all values of magnetic field from 1.5 to 6 kG, the largest available, and the observed decays are independent of field with two exceptions discussed later. At 6 kG, however, the Zeeman splitting between the two transitions is 0.13 cm^{-1}, which is approximately equal to the optical linewidth of the R_1 line.[16] Thus, we made a direct check

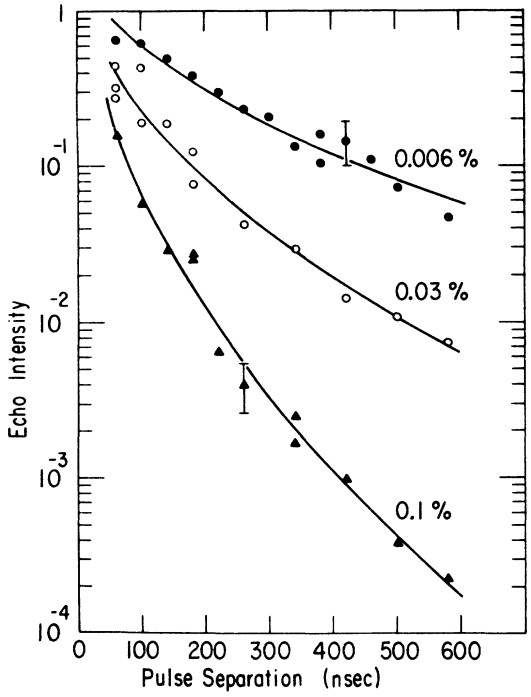

FIG. 4. Photon-echo decay for the $(-\frac{1}{2} \rightarrow -\frac{1}{2})$ transition in the three lowest-concentration samples. Intensity is arbitrarily shifted from one sample to the next for clarity in presentation. Solid curves are least-squares fits to a decay of the form $I = I_0 \exp(-K\tau^{1/2})$, where τ is the pulse separation. A magnetic field of 6 kG for 0.03 and 0.1% and 2.7 kG for 0.006% is parallel to the c axis of the samples. Typical error is shown.

of the resonance conditions at 6 kG by tuning the narrow ($\Delta\bar{\nu} \cong 0.02$ cm^{-1}) laser-emission line across the absorption lines of the sample while monitoring the echo intensity. Under our experimental conditions the laser emission occurs principally from $^2E(\bar{E})(\pm\frac{1}{2}) \rightarrow {}^4A(\pm\frac{3}{2})$, with some weak emission terminating on $^4A(\pm\frac{1}{2})$. The results shown in Fig. 3 were obtained by pumping on the liquid-nitrogen bath to which the laser crystal was connected by a copper rod. Figure 3(a) was obtained with the laser pulsed once every 10 sec—our usual rate for the photon-echo-decay measurements. For the data of Fig. 3(b) the laser temperature was raised by double pulsing the laser according to the following sequence: pulse No. 1 at $t = 0$, pulse No. 2 at $t = 2$ sec, and this pattern repeated every 10 sec. Only pulse No. 2 was photographed. Comparing the two sets of data, we estimate the laser-rod temperature to be about 4 °K higher for the data of Fig. 3(b). From the known 0.13-cm^{-1} splitting of the two transitions at 6 kG, the frequency shift of the laser in this temperature range may be estimated as approximately 0.017 cm^{-1}/°K. For most of the decay measurements the liquid-nitrogen bath was maintained at 77 °K; consequently we conclude that at 6 kG the laser frequency was approximately 0.06 cm^{-1} from the peak of each of the two Zeeman components, and for the plane-polarization results both transitions were simultaneously excited with nearly equal amplitudes.

C. Experimental Results

The principal results of the echo-intensity–vs–pulse-separation measurements are shown in Figs. 4–7 for both the $(-\frac{1}{2} \rightarrow -\frac{1}{2})$ and $(+\frac{1}{2} \rightarrow +\frac{1}{2})$ transitions, and for six ruby samples ranging from 0.006 to 1.2% Cr concentration. The solid curve in each case is a fit of the data to a decay of the form $I = I_0 \exp(-K\tau^{1/2})$. The data for 0.1% are probably the best test of the τ dependence of the decay and show good agreement with this shape for decays which span three orders of magnitude over a range of ~ 600 nsec in pulse separation. Although early measurements,[11] over the range $30 \leq \tau \leq 270$ nsec, appeared to be consistent with exponential decays $I = I_0 e^{-\tau/T}$, the present data with pulse separations up to 580 nsec clearly indicate the slower decay at long pulse separations characteristic of the $\exp(-K\tau^{1/2})$ shape. The data for other concentrations appear also to fit rather well the $\exp(-K\tau^{1/2})$ shape; although in the high-concentration samples (0.55–1.2%) the rapid decay prevents a careful test of the τ dependence. For the latter samples, the

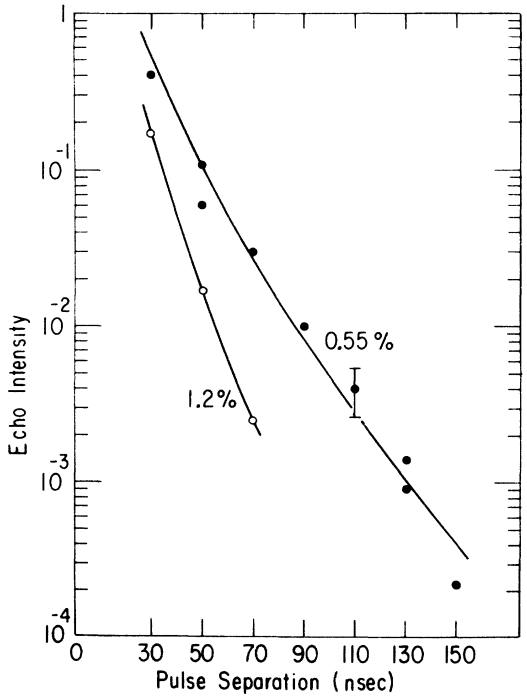

FIG. 5. Photon-echo decay for the $(-\frac{1}{2} \rightarrow -\frac{1}{2})$ transition with magnetic field of 6 kG parallel to the c axis for both the 0.55 and 1.2% samples. Other parameters are the same as for Fig. 4.

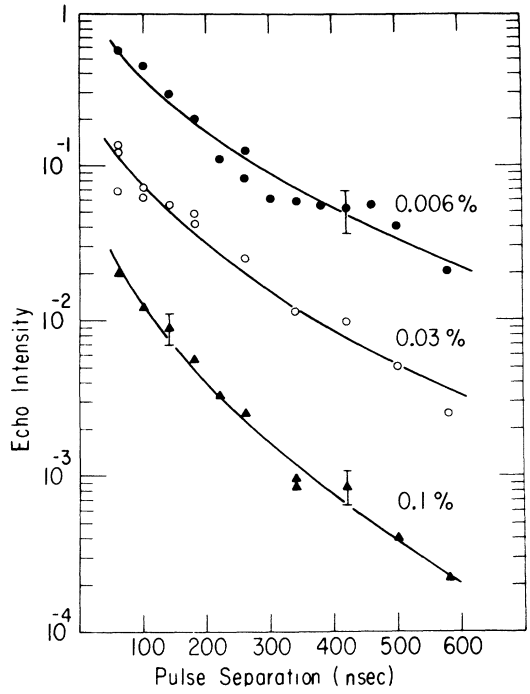

FIG. 6. Photon-echo decay for the $(+\frac{1}{2}\rightarrow+\frac{1}{2})$ transition with magnetic fields of 6 kG for 0.03 and 0.1% samples and 2.7 kG for 0.006% sample applied parallel to the c axis. Other parameters are the same as in Fig. 4.

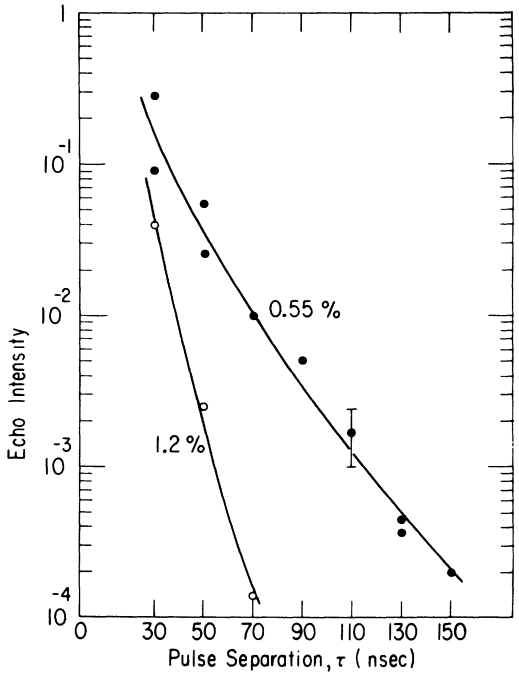

FIG. 7. Photon-echo decay for the $(+\frac{1}{2}\rightarrow+\frac{1}{2})$ transition in the two highest-concentration samples with a magnetic field of 6 kG parallel to the c axis of each. Other parameters are the same as in Fig. 4.

simple exponential dependence on the pulse separation τ also fits.

Further decay measurements were made at magnetic fields ranging from 1.5 to 6 kG which show that the decay is independent of the strength of the external magnetic field in this region, except in the immediate vicinity (± 100 G) of the ground-state level crossings. Near both the 2.06- and 4.12-kG ground-state level crossings, photon echoes from a crossing state, either $-\frac{1}{2}$ or $+\frac{1}{2}$ which cross the $^4A(+\frac{3}{2})$ state at 2.06 and 4.12 kG, respectively, show a greatly modified decay which can be understood on the basis of Cr-Al interactions[17] and will not be discussed here. However, we observe an increased decay also in the $+\frac{1}{2}$ *noncrossing* state at 2.06 kG which is concentration dependent and, as seen in Fig. 8, has roughly the same shape as the decays observed at 6 kG.

Figure 9, curve (a), summarizes the experimental data for Figs. 4–7 and shows the concentration dependence of the decay constant K. We observe that, with the possible exception of the 0.1% sample, both circularly polarized photon echoes for a given

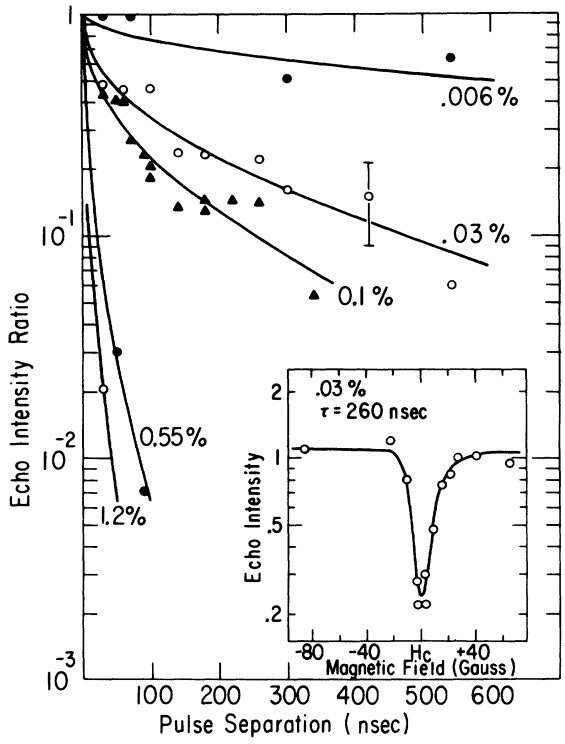

FIG. 8. Additional decay observed at 2.06 kG for the $(+\frac{1}{2}\rightarrow+\frac{1}{2})$ transition. Each point is the ratio of the echo intensity of the minimum at 2.06 kG to the intensity 200 G or more away. A typical observation, shown in the insert, is made by sweeping the magnetic field through the $H_c = 2.06$ kG region. Solid curves are a fit of the data to an additional decay of the form $\exp(-K'\tau^{1/2})$. All curves are assumed to pass through unity at $\tau = 0$.

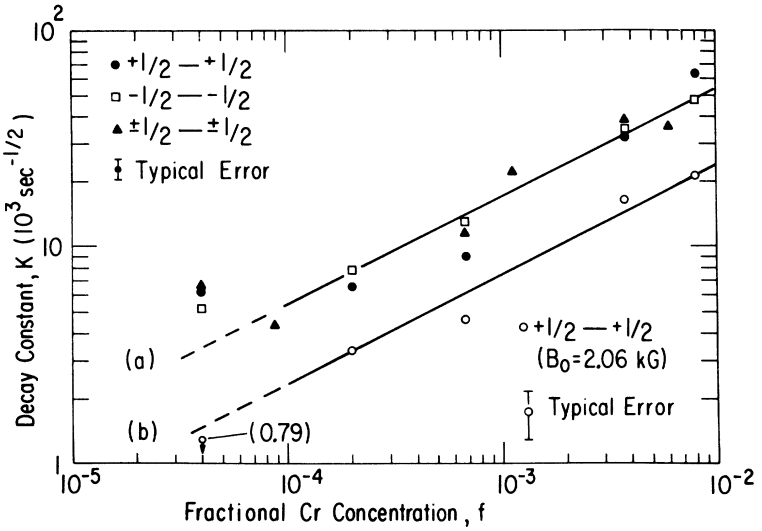

FIG. 9. Decay constants of the curves of Figs. 4–7, and of other decay measurements using plane polarization on 90° c axis samples with a magnetic field of 3 kG, plotted as a function of fractional Cr concentration f. The straight lines indicate the expected $f^{1/2}$ concentration dependence. The open circles give the decay constant of the additional decay observed in the $(+\frac{1}{2} \rightarrow +\frac{1}{2})$ transition at 2.06 kG (see Fig. 8). The error bars represent 90% confidence limits for the least-squares fits to the decay constants.

sample exhibit nearly identical decay constants. Thus we have also included in this figure the plane-polarization results obtained on the 90° c-axis samples. Figure 9, curve (b), shows the increased decay constants taken from Fig. 8 plotted as a function of concentration. The increased decay constant is the difference between the constants measured at 2.06 kG and, e.g., at 6 kG. A concentration dependence of $n^{1/2}$ for the decay constants of both curves a and b is clearly indicated with a significant deviation occurring only in the lightest sample studied 0.006% and for the $(+\frac{1}{2} \rightarrow +\frac{1}{2})$ transition in the 0.1% sample. The approximately linear concentration dependence of the decay constant derived from earlier data[11] covering a smaller range of concentrations and pulse separations followed from the assumed $e^{-\tau/T}$ shape for the decay. Numerical tests for "goodness of fit" show little difference between the $\exp(-K\tau^{1/2})$ and $e^{-\tau/T}$ shapes for the dark samples (0.55–1.2%). However, for the lighter samples (0.006–0.1%) the χ^2 value or equivalently the variance of the fit S^2 is in most cases about a factor of 2 larger for the $e^{-\tau/T}$ fit than for the $\exp(-K\tau^{1/2})$ fit, where $S^2 = \sum_i [y_i - f(\tau_i)]^2/(n-p)$ with y_i as the datum point corresponding to τ_i, $f(\tau)$ is the functional form to be fitted, n is the number of data points, and $p = 2$ equals the number of parameters in the fit. For example, the 0.1% sample yields $S^2(-\frac{1}{2} \rightarrow -\frac{1}{2}) = 0.078$ and $S^2(+\frac{1}{2} \rightarrow +\frac{1}{2}) = 0.035$ for the $\exp(-K\tau^{1/2})$ fit whereas $S^2(-\frac{1}{2} \rightarrow -\frac{1}{2}) = 0.178$ and $S^2(+\frac{1}{2} \rightarrow +\frac{1}{2}) = 0.071$ for the $e^{-\tau/T}$ fit. The principal results shown here, namely, the $\exp(-K\tau^{1/2})$ shape and the $n^{1/2}$ concentration dependence for both the normal decay and the increased decay at 2.06 kG, can be accounted for on the basis of the Cr-Cr interaction model described below.

Using the technique of temperature tuning of the laser frequency described above, we measured the decay of photon echoes arising from various parts of the inhomogeneously broadened optical line of the 0.03% sample. Identical decays were observed with the laser tuned within ~0.06 cm^{-1} of the line center of either transition or as far as 0.18 cm^{-1} into the short-wavelength tail of the $(-\frac{1}{2} \rightarrow -\frac{1}{2})$ transition. However, with the laser tuned approximately 0.13 cm^{-1} to the long-wavelength (red) side of the $(+\frac{1}{2} \rightarrow +\frac{1}{2})$ transition, a significantly slower decay was observed as shown in Fig. 10. The difficulty of raising the laser temperature still higher prevented our tuning the laser farther into the wing of the $(+\frac{1}{2} \rightarrow +\frac{1}{2})$ line or into the long-wavelength tail of the $(-\frac{1}{2} \rightarrow -\frac{1}{2})$ line to see if the effect appears in both transitions. This anomalously slow decay is discussed further in Sec. IV where it is interpreted in terms of an inhibited spin-flip decay mechanism.

III. PHOTON-ECHO DECAY DUE TO SPIN FLIPS

In this section we analyze the photon-echo decay which may be expected on the basis of magnetic dipole-dipole interactions between Cr ions and show that Cr-Cr spin-flip mechanisms account for the principal features of the photon-echo decays discussed above.

Our analysis of the photon-echo decay due to Cr-Cr magnetic interactions follows generally the approach used to describe the decay of spin echoes in solids. Thus, we shall distinguish two spin-flip contributions to the photon-echo decay. The *first* is a *direct* contribution in which *the spin of an echo-producing ion flips* some time between the first pulse and the echo and, consequently, the ion is completely lost from the echo. The *second* contribution[18–20] is an *indirect* effect which occurs when the spin of the echo ion does *not* flip but *other spins in the vicinity flip* and thus give rise to local

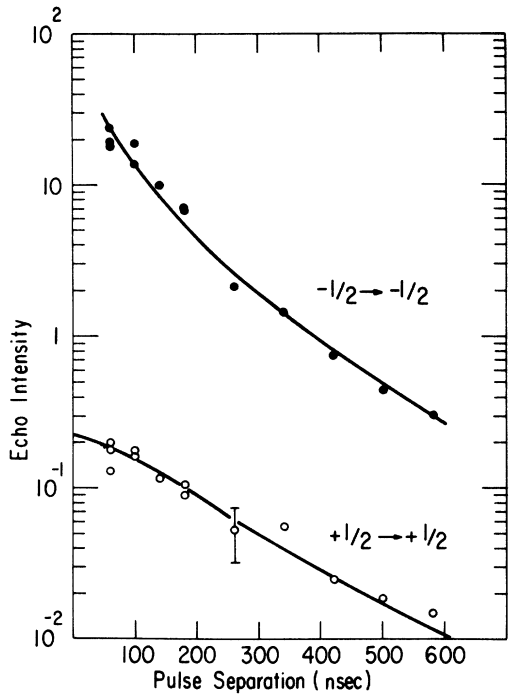

FIG. 10. Photon-echo decay for the 0.03% sample, at a field of 6 kG taken with the laser tuned approximately to the center of the $(-\frac{1}{2}\rightarrow-\frac{1}{2})$ transition and approximately 0.13 cm^{-1} into the long-wavelength tail of the $(+\frac{1}{2}\rightarrow+\frac{1}{2})$ transition. Solid curve for the $(-\frac{1}{2}\rightarrow-\frac{1}{2})$ data is consistent with those of Figs. 4 and 6 for 0.03%. The solid curve for the $(+\frac{1}{2}\rightarrow+\frac{1}{2})$ data is appropriate for diffusion decay as discussed in the text. Intensities of the two polarizations relative to each other are accurate.

magnetic field fluctuations at the nearby echo ion. These produce small fluctuations of the optical frequency and a consequent gradual loss of "phase memory" of the echo ions which causes the echo to decrease in size as the pulse separation increases.

A. General Formalism

We shall describe the effects of spin-flip mechanisms on the photon echo through a density-matrix approach with an emphasis on only those parts essential to understanding the echo decay. Assuming that the interaction with the external magnetic field is large compared to the magnetic interactions between the spins of the Cr ions, then the spins of the ions will be uncorrelated and the density matrix of the collection of N ions, which in the general case is a $2N\times 2N$ matrix, may be written as a direct product of N 2×2 matrices, each describing one atom,[21] that is,

$$\rho^{(2N)}(t)=\prod_{i=1}^{N}\rho^{(2)}(t)\,. \tag{1}$$

The electronic states of the echo ions are highly correlated because of the coupling to a common radiation field, and it is this correlation which gives rise to the superradiant echo state. These correlations are treated in detail by Dicke[22] and in Ref. 1 and are essential in considering, e.g., the intensity and directionality of the echo emission. However, the spin-spin interactions are not greatly affected by the laser pulses since only a small fraction of the Cr ions in the inhomogeneously broadened absorption line "see" the narrow linewidth laser pulses. Thus the predominant magnetic effects arise from the spins of the 95% or more[16] of the ions in the ground state which remain unaffected by the optical pulse and therefore with uncorrelated spin states.

If $\vec{p}_i$ is the electric dipole moment operator of the ith Cr ion, the radiated echo intensity may be obtained in the usual way[1] as

$$I_{\text{echo}}\sim\left|\sum_i \mathrm{Tr}[\vec{p}_i\rho_i(2\tau)]\right|^2$$

$$\sim N^2\left|\langle \mathrm{Tr}[\vec{p}\rho(2\tau)]\rangle_{\text{av}}\right|^2\,. \tag{2}$$

In the second step we have omitted terms of order N which describe the incoherent spontaneous emission of the system. The average must be taken over all echo ions because the time development of the individual density matrices varies due to the random nature of the spin flips and also according to the particular local magnetic environment; the evaluation of this average constitutes the essence of our calculation. The time dependence of the density matrix is given by the equation of motion[23]

$$\frac{d\rho_i(t)}{dt}=-\frac{i}{\hbar}\left[\mathcal{H}_i,\rho_i(t)\right]-\tfrac{1}{2}\{\Gamma_i,\rho_i(t)\}\,, \tag{3}$$

with the solution

$$\rho_i(t)=\exp\left(-\frac{i}{\hbar}\,\mathcal{H}_i t-\tfrac{1}{2}\Gamma_i t\right)\rho(0)\exp\left(+\frac{i}{\hbar}\,\mathcal{H}_i t-\tfrac{1}{2}\Gamma_i t\right), \tag{4}$$

where the curly brackets represent an anticommutator. $\mathcal{H}_i$ is the single-ion Hamiltonian with the form

$$\mathcal{H}_i=\mathcal{H}_i^0-\vec{p}_i\cdot\vec{E}(t)-\vec{\mu}_i\cdot\vec{B}_0-\vec{\mu}_i\cdot\vec{B}_i(t)\,, \tag{5}$$

where $\mathcal{H}_i^0$ describes the energy levels of the Cr ion in the crystalline field; $\vec{E}(t)=\vec{\mathcal{E}}(t)\cos(\omega t)$ is the electric field of the laser pulses with the slowly varying amplitude $\vec{\mathcal{E}}(t)$; $\vec{B}_0$ is the external magnetic field; and $\vec{B}_i(t)=\sum_{j\neq i}[\vec{\mu}_j-3(\vec{\mu}_j\cdot\hat{r}_{ij})\hat{r}_{ij}]/r_{ij}^3$ is the sum of the dipolar fields of the neighboring magnetic moments μ_j. The decay matrix Γ_i may be written as

$$\Gamma_i=\begin{pmatrix}\gamma_i^a & 0\\ 0 & \gamma_i^b\end{pmatrix} \tag{6}$$

and separately describes the loss of ions from the

excited state a and ground state b of the two-level echo system which occurs if an echo ion experiences a spin flip. In the event of such a spin flip the ion remains in an excited or ground state but has a different magnetic quantum number and is no longer coupled to the same circularly polarized electromagnetic field. Consequently, it is lost from the echo system. The off-diagonal elements of Γ_i are taken to be zero since the spontaneous emission rate is very slow $\sim 4\times 10^{-3}$ sec.

In order to retain the analysis in terms of a 2×2 density matrix and yet include the effects of other spins, the single-ion Hamiltonian [Eq. (5)] must be time dependent. This is introduced through the local field $\vec{B}_i(t)$, whose time dependence must be explicitly given. We thus avoid considering $\vec{\mu}_j$ and $\vec{B}_i$ as operators. Furthermore, with a strong external field in the z direction, we need consider only the time-dependent changes of μ_j^z and B_i^z since the transverse components of the local field produce a negligible energy shift.

Introducing the "Dicke operators" R_1, R_2, R_3, optical analogs of the Pauli spin matrices,[22] the single-ion Hamiltonian may be written

$$\mathcal{H}_i(t) = \hbar\omega_i^0 R_3 + (\mu_z' - \mu_z)[B_0 + B_i^z(t)]R_3 + \tfrac{1}{2}(\mu_z' - \mu_z)B_i^z(t)I - \vec{\mathfrak{p}}\cdot\vec{\mathcal{E}}(t)e^{i\omega t}R_2 + \text{H.c.}, \quad (7)$$

where $\hbar\omega_i^0 - E_i^a - E_i^b$ is the optical energy,

$$R_2 = \frac{1}{2}\begin{pmatrix} 0 & -i \\ i & 0 \end{pmatrix}, \quad R_3 = \frac{1}{2}\begin{pmatrix} 1 & 0 \\ 0 & -1 \end{pmatrix}, \quad I = \begin{pmatrix} 1 & 0 \\ 0 & 1 \end{pmatrix},$$

and μ' and μ are, respectively, the excited- and ground-state magnetic moments of the Cr ion. The decay matrix Γ_i may similarly be rewritten

$$\Gamma_i = \tfrac{1}{2}(\gamma_i^a + \gamma_i^b)I + (\gamma_i^a - \gamma_i^b)R_3 . \quad (8)$$

Making the usual assumption[1] that the laser pulses are strong and very near resonance, i.e., $\omega - \omega_i^0 \ll \mathfrak{p}\mathcal{E}/\hbar$, the density matrix for $t > \tau$ may be written

$$\rho(t) = T_2\Theta_2 T_1\Theta_1\rho(0)\Theta_1^{-1}T_1^{-1}\Theta_2^{-1}T_2^{-1} . \quad (9)$$

The pulse operator Θ is given by

$$\Theta(\Delta\tau) = \exp(-i\omega\Delta\tau R_3)\exp(-i\theta R_2)\exp(+i\omega\Delta\tau R_3) , \quad (10)$$

where

$$\theta = \frac{\mathfrak{p}}{\hbar}\int_0^{\Delta\tau}\mathcal{E}(t')\,dt' ,$$

with $\Delta\tau$ as the pulse width. The time evolution operator in the absence of a pulse is

$$T(t) = \exp\{-i[\omega_i^0 t + \hbar^{-1}\int_0^t(\mu_z' - \mu_z)B_i^z(t')\,dt']R_3 + \tfrac{1}{2}[\hbar^{-1}(\mu_z' + \mu_z)\int_0^t B_i^z(t')\,dt']I + \tfrac{1}{4}(\gamma_i^a + \gamma_i^b)I + \tfrac{1}{2}(\gamma_i^a - \gamma_i^b)R_3\} . \quad (11)$$

The identity operator I commutes with both R_2 and R_3, and thus the imaginary coefficient of I collapses to unity with the corresponding term of T_1^{-1} when the trace is taken. Defining the quantities

$$\omega_0'^i = \omega_0^i + \hbar^{-1}(\mu_z' - \mu_z)[B_i^z(0) + B_0] \quad (12)$$

and[19]

$$s(t) = +1 \quad \text{for } 0 \le t \le t$$
$$= -1 \quad \text{for } t > t , \quad (13)$$

we obtain for the relevant terms of the expectation value of the dipole moment operator

$$\langle\vec{\mathfrak{p}}(t)\rangle_{\text{av}} = \langle\text{Tr}[\vec{\mathfrak{p}}\rho(t)]\rangle_{\text{av}} \sim \sin(\theta_1/2)\cos(\tfrac{1}{2}\theta_1)\sin^2(\tfrac{1}{2}\theta_2) \times \langle\cos[\omega_0'(t-2\tau)]\rangle_{\text{av}} Q(t)R(t) , \quad (14)$$

where

$$Q(t) = \langle\exp[-\tfrac{1}{2}(\gamma^a + \gamma^b)t]\rangle_{\text{av}} \quad (15)$$

and

$$R(t) = \langle\cos\{\hbar^{-1}\int_0^t dt' s(t')(\mu_z' - \mu_z) \times [B^z(t') - B^z(0)]\}\rangle_{\text{av}} . \quad (16)$$

The inhomogeneous optical linewidth gives a spread in ω_0' within the crystal, and thus the average of the $\cos[\omega_0'(t-2\tau)]$ term in Eq. (14) is zero except at $t = 2\tau$. As a result, the averages for $Q(t)$ and $R(t)$ are to be taken with $t = 2\tau$. Since the echo intensity is proportional to $|\langle\vec{\mathfrak{p}}(2\tau)\rangle_{\text{av}}|^2$, the echo decay is proportional to Q^2R^2. The factor Q^2 accounts for the decay due to the direct spin-flip effect and shows the relationship to the spin-flip rates of the echo ions in both the ground and excited states. The factor R^2 accounts for the indirect, frequency diffusion effects of spin flips and shows how this decay requires a time-varying local magnetic field at the echo ions. In addition, Eq. (16) shows how this photon-echo-decay factor depends on the *difference* between the excited-state and ground-state magnetic moments of the echo ion. Thus, for the ruby transitions which we studied

$$\mu' - \mu = m\mu_B(g' - g) = \pm\tfrac{1}{2}\mu_B(2.44 - 1.98) = \pm 0.23\mu_B , \quad (17)$$

where μ_B is the Bohr magneton. In contrast, spin-echo transitions generally have $\Delta m = +1$, so that $\mu' - \mu = g\mu_B$. Hence the frequency diffusion decay may be considerably suppressed for photon echoes. The evaluation of the averages over all echo ions, indicated in Eqs. (15) and (16), will now be performed assuming a random statistical distribution of Cr ions.

B. Direct Spin-Flip Decay Factor

If the spin-flip rates γ^a and γ^b were associated with spin-lattice relaxation, the average of the decay factor $Q(t)$ would trivially yield a photon-echo decay of $Q^2(2\tau) = \exp[-(\gamma^a + \gamma^b)2\tau]$, since the lattice relaxation rate would be the same for all ions. However, in ruby at liquid-helium temperatures, spin-lattice relaxation times are very long ($\sim 10^{-2}$ sec)[24] so that for concentrations of interest in this experiment spin-spin relaxation dominates. This relaxation rate is strongly dependent on the local magnetic environment, and when the decay factor is appropriately averaged we shall obtain a photon-echo decay of the form $\exp(-K\tau^{1/2})$. The decay constant K is found to be proportional to the *square root* of the Cr concentration when dipolar interactions are assumed.

The following calculation can be simplified somewhat by setting the excited-state spin-flip rate γ^a equal to zero. This may be justified for strong external magnetic fields by noting that because of the difference in g factors between the Cr ground state ($g = 1.98$) and excited state ($g' = 2.44$), an excited-state spin is not resonant with a ground-state spin and, therefore, they cannot experience mutual flip flops. Since only a small fraction of the ions (of the order of 5% or less) is excited by the laser pulses,[16] the excited-state spin-flip rate is correspondingly suppressed. Thus we neglect the spin-flip rate γ^a and drop the superscript on γ^b which is no longer needed. We write the total ground-state spin-flip rate for an ion i as

$$\gamma_i = \sum_j \frac{2\pi}{\hbar} |V_{ij}|^2 I_{ij}(E) , \tag{18}$$

where $I_{ij}(E) = \int g_i(E) g_j(E)\, dE$, and $g_i(E)$ and $g_j(E)$ are the normalized *magnetic* line-shape functions for ions i and j, respectively. For dipolar interactions, the matrix element V_{ij} is given by

$$V_{ij} = \langle m_i', m_j' | [\vec{\mu}_i \cdot \vec{\mu}_j - 3(\vec{\mu}_i \cdot \hat{r}_{ij}) \times (\vec{\mu}_j \cdot \hat{r}_{ij})]/r_{ij}^3 | m_i m_j \rangle , \tag{19}$$

where $\vec{\mu}_i = g\mu_B \vec{S}_i$ and $\vec{\mu}_j = g\mu_B \vec{S}_j$ are the magnetic moments of ions i and j separated by the distance $\vec{r}_{ij}$. Matrix elements of the form

$$V_{ij} = \tfrac{1}{4}[(g\mu_B)^2/r_{ij}^3](1 - 3\cos^2\theta_{ij}) \times \langle m_i \pm 1, m_j | S_i^+ S_j^- + S_i^- S_j^+ | m_i, m_j \pm 1 \rangle \tag{20}$$

will be allowed for all values of external magnetic field if $m_i = m_j$, but the transitions do not conserve energy if $m_i \neq m_j$ because of the Cr ground-state quadrupolar splitting. Taking the absolute square of these matrix elements and averaging over the four equally probable values of m_j, we obtain

$$|V_{ij}|_{\rm av}^2 = [(g\mu_B)^4/r_{ij}^6]\, a(1 - 3\cos^2\theta_{ij})^2 , \tag{21}$$

where $a = \frac{25}{64}$ for $m_i = \pm\frac{1}{2}$, and $a = \frac{9}{64}$ for $m_i = \pm\frac{3}{2}$.

Knowledge of γ_i gives us the echo-decay factor characterizing ions which have neighboring ions j in a specific set of lattice positions defined by r_{ij}, θ_{ij}, φ_{ij}, relative to ion i. An average of the decay factor must then be taken over all such possible configurations of neighboring ions frozen in when the crystal was grown. This may be done by assuming a random, statistical distribution of ion locations according to a procedure outlined by Anderson,[25,26] which we briefly summarize. For a statistical distribution, the probability for finding a spin in the volume element $dV_j = r_{ij}^2\, dr_{ij} \times d(\cos\theta_{ij}) d\varphi_{ij}$ is just dV_j/V where V is the total crystal volume. Thus the probability of obtaining the spin-flip rate γ_i is $\Pi_{j=1}^N (dV_j/V)$ or just the probability for finding N spins at specified locations (r_{ij}, θ_{ij}, φ_{ij}). To average over the entire crystal, one allows each dV_j to roam over all lattice sites or in the continuum limit, one integrates each dV_j over the crystal. Therefore,

$$Q(2\tau) = \int \frac{dV_1}{V} \cdots \int \frac{dV_i}{V} \cdots \int \frac{dV_N}{V} e^{-\gamma_i \tau} = \left[\int \frac{dV}{V} \exp\left(-\tau \frac{2\pi}{\hbar} |V|_{\rm av}^2 I(E)\right)\right]^N . \tag{22}$$

This last result follows if we assume that $I_{ij}(E)$ is independent of i and j in which case each of the N integrals is identical. We defer to the end of this section a discussion of the validity of this assumption. By a slight manipulation, Eq. (22) becomes

$$Q(2\tau) = \left\{1 - \frac{1}{N}\int \frac{dV}{v}\left[1 - \exp\left(-\tau \frac{2\pi}{\hbar} |V|_{\rm av}^2 I(E)\right)\right]\right\}^N = e^{-\chi/v} = e^{-n\chi} , \tag{23}$$

where $v^{-1} = n =$ the density of Cr ions, and

$$\chi = \int_0^{2\pi} d\varphi \int_{-1}^{+1} d(\cos\theta) \times \int_0^{\infty} r^2 dr \left[1 - \exp\left(-\tau \frac{2\pi}{\hbar} |V|_{\rm av}^2 I(E)\right)\right] . \tag{24}$$

The effect of extending the radial integral from the crystal boundary to infinity should have negligible effect since $|V|^2 \sim r^{-6}$.

Using Eq. (21) for $|V|^2$, the expression for χ may be evaluated using the following change of variable:

$$x = r^3 \hbar^{1/2}/[2\pi(g\mu_B)^4\, a(1 - \cos^2\theta)^2\, I(E)\tau]^{1/2} . \tag{25}$$

Thus, one obtains

$$\chi = \tfrac{2}{3}\pi[2\pi\tau(g\mu_B)^4\, aI(E)/\hbar]^{1/2} JL , \tag{26}$$

where

$$J=\int_{-1}^{+1} d(\cos\theta)\,|1-3\cos^2\theta| = 8/(3\sqrt{3}) \qquad (27)$$

and

$$L=\int_0^{\infty} dx[1-\exp(-x^{-2})]\cong 1.78\ . \qquad (28)$$

The resulting photon-echo-decay factor for an echo arising from an $m=\pm\frac{1}{2}$ ground state is

$$Q^2(2\tau)=\exp\{-36(g\mu_B)^2 n\tau^{1/2}[I(E)/\hbar]^{1/2}\}\ . \qquad (29)$$

For an estimate of the overlap integral $I(E)$ we shall use the reciprocal of the magnetic linewidth which may be calculated by a statistical technique similar to that described above. The full width at half-maximum (FWHM) for a spin-$\frac{3}{2}$ system is approximately[26]

$$\Delta E=h\Delta\nu_{\mathrm{FWHM}}=15(g\mu_B)^2 n\ . \qquad (30)$$

Writing the Cr density in ruby as $n=fn_0$, where $n_0=4.7\times10^{22}$ cm^{-3} is the density of Al atoms in pure sapphire, the photon-echo-decay factor becomes explicitly

$$Q^2(2\tau)=\exp[-11\times10^5(f\tau)^{1/2}]\ , \qquad (31)$$

where f is the fractional Cr concentration, i.e., (the number of Cr)/(number of Al plus number of Cr).

Equation (31) exhibits explicitly the $\tau^{1/2}$ dependence of the exponential decay which we anticipated with the solid curves in Figs. 4–7. In addition, Eq. (31) shows the $f^{1/2}$ concentration dependence of the decay constant experimentally observed in Fig. 9. Furthermore, the calculated value for the decay constant, $K=11\times10^5 f^{1/2}$, is remarkably close to the experimental value of $(5.4\pm0.5)\times10^5 f^{1/2}$ considering the several simplifying assumptions we have made and our rough estimate of the overlap integral.

A physical interpretation of the flattening of the decay curves at large pulse separations, which is characteristic of the $\exp(-K\tau^{1/2})$ shape, is readily given in terms of the statistical variation of local magnetic environments in the crystal. Those ions with higher than average densities of neighboring Cr ions give rise to the rapid initial photon-echo decay, but at large pulse separations the only ions left to contribute to the echo belong primarily to neighborhoods with lower than average densities of Cr spins and, therefore, with smaller spin-flip rates. Thus each type of magnetic environment contributes a characteristic slope to the photon-echo decay. The composite of all environments yields the observed curve with a smoothly varying tangent. The exact $\tau^{1/2}$ dependence which is calculated is a consequence of (i) the dipole-dipole nature of the interaction and (ii) the assumption of a random, statistical placement of Cr ions. For example, if the interaction were of quadrupole-quadrupole type then $|V|^2\sim 1/r^8$ and inspection of Eqs. (24)–(26) reveals that an $\exp(-K\tau^{3/8})$ shape would be predicted. The technique of averaging over all magnetic environments is applicable even if the distribution of ions in the crystal is not random. If clustering occurs then the probability for finding a spin in the volume element dV_j may be written as $f(r_j)\,dV_j/V$. For example, if $f(r_j)=1/r_j$ the integration variable in the radial integral of Eq. (24) is modified from $r^2dr=\frac{1}{3}d(r^3)$ to $\frac{1}{2}d(r^2)$. Consequently, one would obtain a decay of the form $\exp(-K\tau^{1/3})$. Similar arguments may be used to examine how the concentration dependence of the decay constant K depends on the form of the interaction or on possible clustering of the Cr ions. All of our data, however, appear to be consistent with a dipole-dipole interaction and a completely random distribution of ions in the lattice.

We now briefly return to discuss the possible effects of the assumptions made earlier. First, the expression for the spin-flip rate γ_i of Eq. (18) ignores possible three-body and higher-order correlations which may become important for large values of r_{ij}. The fact that the calculated decay agrees well with the observed decay indicates that such correlations are not important for this experiment. Second, the assumption in Eq. (22) that the overlap integral is a constant oversimplifies the situation, but since the spin-resonance line shows little strain broadening,[27] Eq. (22) should be a good approximation to an average overlap except for very low concentrations where Cr-Al interactions dominate the experimental linewidth.[27] Below about 0.01%, the experimental spin-resonance linewidth is constant, and thus $I(E)$ is also constant, independent of concentration, and hence, the decay constant K will be proportional to f rather than $f^{1/2}$, i.e., the decay constant due to Cr-Cr spin flips is expected to fall off more rapidly with decreasing concentration in this region. Experimentally we observe in the 0.006% sample a decay constant larger than expected even on an $f^{1/2}$ extrapolation which probably indicates the presence of a residual decay mechanism at low concentrations, perhaps due to Cr-Al interactions. Third, the radial integral in Eq. (24) has as its lower limit $r=0$, and consequently, the slope of the echo decay at $\tau=0$ is $(dQ^2/d\tau)_{\tau=0}=-\infty$. This ignores the fact that there is a minimum distance r_{min} for which Eq. (18) is valid. This problem is similar to that encountered in calculating the spin-resonance line shape in dilute spin systems in which case a cutoff is often introduced in the wings of the frequency spectrum.[26,28] Kittel and Abrahams use a cutoff frequency of $\alpha=2.2(g\mu_B)^2/ha^3$, where a is the simple-cubic-lattice constant. In ruby there is evidence of fairly strong exchange interactions extending to a distance of $r\approx5.7$ Å. Using this radius

as a lower limit, the cutoff frequency becomes $\alpha \approx 5\times10^{8}$ sec^{-1} and identifying α with a maximum spin-flip rate γ_{max} it is clear from the discussion of the preceding paragraph that the limiting slope of the photon-echo decay should be $(dQ^2/d\tau)_{max} = -\gamma_{max} = -2\pi\alpha$. The effect of the cutoff would not be observable for the pulse separations we have used, but we emphasize that the $\exp(-K\tau^{1/2})$ curve is not expected to hold exactly as τ is extrapolated to zero, and the deviation might be observed by using much smaller pulse widths and pulse separations. Extrapolation of the echo-decay curves is further discussed in the last part of Sec. IV.

C. Spectral-Diffusion Decay Factor

Frequency diffusion has been shown to be a dominant decay mechanism for spin echoes in many cases.[18–20,29] In this section, we shall examine whether and under what circumstances this decay mechanism may be important for photon echoes in ruby. To describe this type of decay in spin echoes, a model of "random-frequency modulation" or "frequency diffusion" was first proposed and applied to the decay of nuclear spin echoes[29] and subsequently extended to randomly diluted spin systems for the case of electron spin echoes.[19,20] In dilute spin systems this model has been very successful in two types of situations: first, in cases where there are two different spin species one of which has a rapid spin-lattice relaxation, and second, in cases where large inhomogeneous broadening of the spin-resonance line allows for a fairly clear distinction between echo-producing spins and others which do not contribute to the echo and which cannot make spin-spin flips with the echo spins but affect them indirectly via the time-dependent local fields. In ruby, however, the spin-resonance line exhibits very little inhomogeneous broadening[27] and no other electron-spin species is present so that the conditions for obtaining a decay dominated by this frequency-diffusion mechanism are not generally satisfied. Also, as discussed at the end of Sec. III A, the frequency-diffusion effects are further suppressed for photon echoes in ruby because of the relatively small change of magnetic moment between ground and excited states. Thus we find for ruby that these frequency- or spectral-diffusion effects are less important for optical transitions than the direct spin-flip effect calculated above.

The computation of the photon-echo-decay factor $R(2\tau)$ due to spectral diffusion will be performed in a manner very similar to that described by Mims[20] for spin-echo decays in dilute spin systems. Our expression [Eq. (16)] for this decay factor may be rewritten

$$R(2\tau) = \langle \mathrm{Re}\exp\{i\hbar^{-1}\int_0^{2\tau} s(t)(\mu'-\mu) \times [B_i(t)-B_i(0)]\,dt\}\rangle_{av}\,, \quad (32)$$

where z subscripts (superscripts) are to be understood on μ', μ, and (B_i), and the real part of the exponential is to be taken. The calculation now proceeds by assuming a simple model[20,29] for the fluctuations of the local magnetic field variable B_i. First it is assumed that $B_i(t)$ has a Gaussian probability distribution, and therefore the quantity

$$\xi_i(2\tau) = \hbar^{-1}\int_0^{2\tau} s(t)(\mu'-\mu)[B_i(t)-B_i(0)]\,dt\,, \quad (33)$$

which is a linear combination of the $B_i(t)$, must also have a Gaussian distribution. Thus the decay factor $R(2\tau)$, averaged only over the subset of ions denoted by the subscript i, which all have the same configuration of neighboring spins (as in Sec. III B), is given by

$$\begin{aligned}\langle R(2\tau)\rangle_i &= \mathrm{Re}\int_{-\infty}^{\infty} d\xi_i \exp[-i\xi_i(2\tau)] \\ &\quad\times \exp[-(\xi_i-\bar{\xi}_i)^2/2\sigma^2]/(2\pi\tau^2)^{1/2} \\ &= \mathrm{Re}\exp[-i\bar{\xi}(2\tau)]\exp[-\tfrac{1}{2}\langle(\xi_i-\bar{\xi}_i)^2\rangle]\,, \quad (34)\end{aligned}$$

where the mean $\bar{\xi}_i(2\tau)$ and the variance $\langle[\xi_i(2\tau) - \bar{\xi}_i(2\tau)]^2\rangle$ are to be evaluated in terms of the assumed behavior of $B_i(t)$.

These averages over a subset of ions with identical environments may be replaced by time averages according to the ergodic theorem,[30] and thus

$$\begin{aligned}\bar{\xi}_i(2\tau) &= \langle\xi_i(2\tau)\rangle_T \\ &= \frac{(\mu'-\mu)}{\hbar}\int_0^{2\tau} s(t)\,\langle B_i(T+t)-B_i(T)\rangle_T\,dt = 0\,, \quad (35)\end{aligned}$$

where the T subscript on the angular brackets denotes an average over time T. Therefore we find

$$\begin{aligned}\langle[\xi_i-\bar{\xi}_i]^2\rangle_T &= \langle\xi_i^2(2\tau)\rangle_T \\ &= \frac{(\mu'-\mu)^2}{\hbar^2}\int_0^{2\tau}d\tau'\int_0^{2\tau}dt''s(t'')s(t') \\ &\quad\times\langle B_i(T+t'')B_i(T+t')\rangle_T\,. \quad (36)\end{aligned}$$

The second assumption of the model is that this autocorrelation function of $B_i(t)$ is typical of a Markoff process[20,29,31] and is therefore given by

$$\langle B_i(T+t'')B_i(T+t')\rangle_T = \sigma_i^2\exp(-\gamma|t''-t'|)\,. \quad (37)$$

A motivation of Eq. (37) and estimates of the quantities γ and σ_i^2 are reserved for the Appendix where we identify γ with an average spin-spin flip rate in the crystal and show that σ_i^2 is related to the size of the local magnetic field fluctuations at ion i.

The integrals in Eq. (36) may now be evaluated to obtain

$$\langle \xi_i^2(2\tau)\rangle_T = 4\frac{(\mu'-\mu)^2}{\hbar^2\gamma^2}\sigma_i^2 C(\tau)\,, \tag{38}$$

where

$$C(\tau) = \gamma\tau - (1-e^{-\gamma\tau}) - \tfrac{1}{2}(1-e^{-\gamma\tau})^2\,. \tag{39}$$

Thus the echo-decay factor for the subset of echo ions with the configuration of neighbor spins denoted by the subscript i is given by the real quantity

$$\langle R(2\tau)\rangle_i = \exp\left(-2\frac{(\mu'-\mu)^2}{\hbar^2\gamma^2}\sigma_i^2 C(\tau)\right). \tag{40}$$

For the quantity σ_i^2, as described in the Appendix, we shall take an upper limit of the form

$$\sigma_i^2 = \tfrac{5}{4}(g\mu_B)^2\textstyle\sum_j (1-3\cos^2\theta_{ij})^2/r_{ij}^6\,. \tag{41}$$

With this form for σ_i^2 it is clear that the average of $\langle R(2\tau)\rangle_i$ over all environments may be performed by the statistical technique of Sec. III B. The result is

$$\langle\langle R(2\tau)\rangle_i\rangle = e^{-nx'}\,, \tag{42}$$

where

$$\chi' = [(\sqrt{10})\pi/3\hbar]g\mu_B(\mu'-\mu)JL[C(\tau)/\gamma^2]^{1/2}\,, \tag{43}$$

and as in Sec. III B,

$$J = 8/(3\sqrt{3}) \tag{27}$$

and

$$L \cong 1.78\,. \tag{28}$$

Using for γ a value equal to one-third of the calculated spin-resonance linewidth, as described in the Appendix, the photon-echo-decay factor due to spectral diffusion is

$$\langle\langle R^2(2\tau)\rangle\rangle = \exp\{-3.2\times10^{10}(f/\gamma)[C(\tau)]^{1/2}\}\,, \tag{44}$$

where f is the fractional Cr-ion concentration.

The quantity $C(\tau)$ of Eqs. (39) and (44) is identical to that obtained in Ref. 20 where a more detailed discussion is given of the shape of the resulting (spin) echo decays and of some of the assumptions involved in the application of this Gauss-Markoff model. We emphasize here that most of our data falls in the transition regime where $\gamma\tau \approx 1$ in which the shape of the decay changes from the limiting forms $\exp[-K(ft)^{3/2}]$ for $\tau \ll 1/\gamma$ to $\exp[-K(ft)^{1/2}]$ for $\tau \gg 1/\gamma$. In this intermediate case the shape appears nearly as a simple exponential in τ, and the decay constant is approximately linear in the concentration f in contrast to the $f^{1/2}$ dependence experimentally observed. In general the predicted spectral-diffusion decays are considerably slower than the observed photon-echo decays in spite of the fact that we have used upper limits for σ_i^2 and γ. A numerical example is given in Sec. IV.

Thus we conclude that generally the photon-echo decay in ruby results from spin flips of echo ions directly, and that the contribution from spectral diffusion is negligible. The experimental evidence of a possible exception to this general behavior is analyzed in Sec. IV.

IV. INTERPRETATION OF OTHER DATA

In this section we shall analyze, in terms of the calculations of Sec. III, the faster decays observed in a noncrossing state at the 2.06-kG level-crossing field and the anomalously slow decay observed in one sample under special laser-sample resonance conditions. Also, in this section we shall compare our photon-echo-decay data with spin-resonance linewidth measurements taken over a similar range of concentrations in ruby, and finally we comment on the behavior of the echo decay in small magnetic fields.

The enhanced decay in the $(+\frac{1}{2} \rightarrow +\frac{1}{2})$ transition at 2.06 kG, as shown in Figs. 8 and 9, is readily understood in terms of the direct spin-flip decay calculated in Sec. III B. The matrix elements of Eq. (20) included only those representing spin flips which are allowed for all values of external magnetic field, but at 2.06 and 4.12 kG other flip-flop transitions do conserve energy. Specifically, at 2.06 kG matrix elements will be allowed of the form

$$\tfrac{3}{4}\sin^2\theta_{ij} \times \langle m_i \pm 1,\ m_j \pm 1 \,|\, S_i^+ S_j^+ e^{-2i\varphi} + S_i^- S_j^- e^{+2i\varphi} \,|\, m_i, m_j\rangle \tag{45}$$

and at 4.12 kG

$$\tfrac{3}{2}\sin\theta_{ij}\cos\theta_{ij} \times \langle m_i \pm 1, m_j \,|\, S_i^+ S_j^z e^{-i\varphi} + S_i^- S_j^z e^{+i\varphi} \,|\, m_i, m_j\rangle\,. \tag{46}$$

These give additional contributions to Eq. (21) of the form

$$|V_{ij}|^2 = [(g\mu_B)^4/r^6](b\sin^4\theta_{ij} + c\sin^2\theta_{ij}\cos^2\theta_{ij})\,, \tag{47}$$

where

$b = \frac{27}{8}$ for $m_i = +\frac{1}{2}$ and $B_0 = 2.06$ kG

$= \frac{27}{16}$ for $m_i = -\frac{1}{2}, +\frac{3}{2}$, and $B_0 = 2.06$ kG

$= 0$ for $m_i = -\frac{3}{2}$

and

$c = \frac{135}{16}$ for $m_i = +\frac{1}{2}, +\frac{3}{2}$, and $B_0 = 4.12$ kG

$= 0$ for $m_i = -\frac{1}{2}, -\frac{3}{2}$.

Consequently, an enhanced decay is expected in these states at these two fields. We have already noted, however, that the crossing states, $-\frac{1}{2}$ and $+\frac{3}{2}$ at 2.06 kG and $+\frac{1}{2}$ and $+\frac{3}{2}$ at 4.12 kG (see Fig.

2), exhibit a greatly modified decay due to Cr-Al magnetic interactions[17] which obscures any additional Cr-Cr spin-flip decay. But the decay of the noncrossing state, $+\frac{1}{2}$ at 2.06 kG, may be used to test the predictions of the spin-flip-decay model. The additional contribution to the decay constant for the $(+\frac{1}{2} \rightarrow +\frac{1}{2})$ transition at 2.06 kG due to the terms of Eq. (47) is easily evaluated by the techniques of Sec. III B, and the decay has the form $\exp(-K'\tau^{1/2})$. The predicted dependence on $\tau^{1/2}$ agrees well with the observations as shown in Fig. 8. The calculated decay constant K' of the increased decay is related to the field-independent decay constant by

$$K'(B_0 = 2.06 \text{ kG}) = 2.54K(B_0 \neq 2.06 \text{ kG}). \quad (48)$$

Thus the total decay constant at 2.06 kG would be $K_{\text{tot}} = 3.54K(B_0 \neq 2.06 \text{ kG})$. This additional decay occurs because of the level-crossing degeneracy so that it vanishes rapidly as the field is raised or lowered from 2.06 kG. Thus the spread in local magnetic fields of 10 G or more, depending on concentration, tends to dimish the amount of increased decay which occurs. Experimentally, as seen in Fig. 9, curve (b), the decay constant at 2.06 kG is enhanced by an average of about 50%. The increased decay also shows the characteristic $n^{1/2}$ concentration dependence typical of this direct spin-flip-decay mechanism. Furthermore, the decay at 2.06 kG is enhanced much less than 50% in the 0.006% sample which confirms the prediction made at the end of Sec. III B that the Cr-Cr spin-flip decay should fall off very rapidly at concentrations below about 0.01%. The increased decay at 2.06 kG in the $(+\frac{1}{2} \rightarrow +\frac{1}{2})$ transition can only result from Cr-Cr effects whereas it is now apparent that there is a residual decay mechanism, not due to Cr-Cr interactions, which accounts for the faster than expected decay observed at 2.7 kG in the 0.006% sample.

Second, we discuss the anomalously slow decay observed for the $(+\frac{1}{2} \rightarrow +\frac{1}{2})$ echo in the 0.03% sample as shown in Fig. 10. We recall that this slower decay is observed only when the laser is tuned to the *long-wavelength* side of the absorption line, whereas the normal decay is observed near the center and on the short-wavelength side. We propose that these ions in the long-wavelength wing of the optical line have Larmor-precession frequencies which also are shifted so that they do not readily undergo flip flops with ions from the main part of the line. This appears plausible from the following argument: It is known that the exchange interactions between near-neighbor Cr ions give rise to optical-pair spectra[6,7] which are shifted to longer wavelengths, so that the spectra of the more distant neighbors, weakly exchange coupled, probably lie within the inhomogeneous R_1 line but shifted slightly toward the red from the line center. There is, in fact, evidence from spin-resonance spectra[8,24] that fairly strong exchange interactions extend to the 10th- or 11th-nearest-neighbor shells corresponding to a distance of about 5.7 Å in ruby. Because the spin-resonance frequencies of these pairs are shifted,[8,24] they do not readily undergo spin flips with single-ion spins. Thus the direct, spin-flip decay for photon echoes arising from these pairs will be inhibited. The indirect, frequency-diffusion decay for these pairs should, however, be nearly unchanged so that this slow decay may result predominantly from the diffusion mechanism. The solid curve for the $(+\frac{1}{2} \rightarrow +\frac{1}{2})$ data in Fig. 10 is a fit of the data to a decay of the form given in Eq. (44). A good fit occurs with $\gamma = 4\times10^6$ sec^{-1} as given in Eq. (A7), but with a decay constant of $5.25f\times10^{10}$ sec which is 65% larger than our calculated *upper estimate*. Although our estimate may be in error by this amount, we cannot preclude the occurrence of even slower decays farther into the wing of the optical line. Lack of sufficient laser tunability also prevented us from determining whether the same effect occurs in the long-wavelength tail of the $(-\frac{1}{2} \rightarrow -\frac{1}{2})$ transition as this interpretation predicts. If, however, our suggestion is correct, this experiment constitutes, to our knowledge, the first evidence of the presence of long-range pair spectra within what is usually interpreted as the inhomogeneously broadened single-ion R_1 line. The data for the 0.1% sample also exhibit a slower decay for the $(+\frac{1}{2} \rightarrow +\frac{1}{2})$ transition and the same explanation as for 0.03% may apply. However, the exact laser-sample resonance was not determined so that a definite conclusion is not possible for this sample. An alternative but less likely explanation of this slow decay requires an assumption that the ions in this part of the line have neighborhoods with a much lower Cr-ion density than characteristic of the rest of the line. An average density roughly equivalent to that of the 0.006% crystal is required. There is, however, no evidence of a concentration-dependent *shift* of the R_1 wavelength, and thus we believe this explanation to be improbable.

Third, we consider the limiting photon-echo-decay behavior in small magnetic fields. The theory of Sec. III assumed the presence of a large static external magnetic field in the sample, and is expected to be applicable as a description of Cr-Cr effects as long as $B_0 \gg B_i \cong \langle \mu/r^3 \rangle_{\text{av}}$. In the darkest sample, 1.2%, the average local field due to neighbor Cr ions is approximately 50 G so that the analysis should be generally applicable for external fields larger than about 500 G. This estimate ignores possible Cr-Al effects, however, which are in fact important at fields of 1 kG and slightly above. A detailed density-matrix analysis of the

effects of the Cr magnetic interaction with the 13 nearest-neighbor Al nuclear spins is to be presented in a subsequent paper.[32]

Finally, since the photon-echo decays are accounted for in terms of magnetic dipolar interactions in the Cr ground state, it is instructive to compare our results with spin-resonance experiments in ruby. If we obtain an approximate decay rate $R=1/T$ from an exponential fit, $e^{-\tau/T}$, to the observed decays, the corresponding linewidth due to spin flip flops is $\Delta\nu = R/2\pi$. The widths inferred in this manner are more than an order of magnitude smaller than measured spin-resonance linewidths[27] for all Cr concentrations we have used. As an example, we would infer a linewidth for our 0.17% sample (atomic-fractional concentration $f=1.1\times10^{-3}$) of $\Delta\nu = 2.6$ MHz. This compares with a spin-resonance linewidth of 26 MHz for a sample with $f=0.92\times10^{-3}$ obtained by Manenkov and Federov.[27] Theoretical linewidth calculations[26,33] indicate, however, that the off-diagonal flip-flop contribution to the spin-resonance linewidth should be about one-third of the total when static inhomogeneous broadening of the line is negligible. The apparent discrepancy results from the use of the exponential decay approximation to the data. We have seen that the $\exp(-K\tau^{1/2})$ form gives a better fit to the photon-echo-decay data but in this case the resulting linewidth is not readily inferred. This simply reflects the fact that one ought not to ascribe the same homogeneous linewidth to the high- as well as the low-density magnetic environments. A more appropriate comparison with spin-resonance linewidths may be time required for the number of participating echo ions to fall to N_0/e, where N_0 is the initial number at $\tau=0$. Since the echo intensity is proportional to N^2, this is equivalent to the time for the echo intensity to fall by a factor of $(1/e)^2$. Denoting this time by T_0 and assuming that the $\exp(-K\tau^{1/2})$ form holds as $\tau\to0$, we obtain

$$\Delta\nu = 1/2\pi T_0 = K^2/16\pi\ , \tag{49}$$

where K is the decay constant of the $\exp(-K\tau^{1/2})$ fit. The values of $\Delta\nu$ obtained in this way are close to the expected one-third of the spin-resonance widths for concentrations above approximately 0.1%. For lower concentrations the comparison is not meaningful since Cr-Al interaction broadening dominates the spin-resonance linewidth. Thus we find, for example, for the 0.17% sample $\Delta\nu = 9.9$ MHz, and Manenkov and Federov obtain $\Delta\nu = 26$ MHz for their $f=0.92\times10^{-3}$ sample. The existence of the cutoff radius discussed at the end of Sec. III B and the consequent maximum (negative) value of the slope of the decay curve does not appreciably affect the $\exp(-K\tau^{1/2})$ extrapolation. The effect is largest for the 1.2% sample where our estimated maximum slope of $R_{max} = -5\times10^{8}$ sec^{-1} is reached at $\tau\cong0.2$ nsec. As a result the estimate of $\Delta\nu$ on the basis of Eq. (49) would be lowered by less than 10% for this sample. Lower-concentration samples reach the limiting slope at even smaller values of τ so that the correction would be less.

Recently, Szabo[9] has used a laser-induced fluorescent-line-narrowing technique to obtain a homogeneous optical linewidth for the $R_1(\pm\frac{1}{2}\rightarrow\pm\frac{1}{2})$ transitions in 0.1% ruby. With a 420-G field parallel to the optic axis, he obtains $\Delta\nu = 32$ MHz which is considerably larger than the upper limit of $\Delta\nu = K^2/16\pi = 2.4$ MHz which we may infer for our 0.1% sample. This comparison suggests that there exists some mechanism, possibly optical spectral diffusion,[6] which is rapid enough to broaden the fluorescence line on the time scale of 4 msec but is too slow to be observed on the 100-nsec time scale of the photon-echo observations.

V. CONCLUSIONS

We have demonstrated first the feasibility of making direct photon-echo–vs–pulse-separation measurements using a single-pulsed laser, plus an optical delay line. These experiments used pulse separations as short as 30 nsec but the technique is capable of much shorter pulse separations since much shorter laser pulse widths are available.[34] This contrasts with miminum pulse widths of about 1 μsec available in spin-echo measurements. It is interesting to note that spin echoes in ruby have been observed in samples of 0.005% Cr concentration but could not be seen[12] in samples of 0.05% Cr so that the important region of concentration for studying Cr-Cr interactions is inaccessible to a spin-echo study, i.e., the decays are too rapid even to *observe* a spin echo.

Second, we have shown that the observed decays, with the exception of the lightest sample, are described very well in terms of a model of spin flips of echo ions due to dipolar spin-spin interactions. The agreement extends over a wide range of sample concentrations and of magnetic fields and is generally applicable to photon echoes from randomly diluted spin systems. Because of this good agreement of the experimental results with the predictions based on magnetic interactions, we conclude that optical energy transfer between single ions must be somewhat slower.[35] This is consistent with an inferred energy-transfer rate between single ions of 10^7 sec^{-1} for 1% ruby[6] compared to our observed photon-echo-decay rate in the 1.2% sample of 1.1×10^{8} sec^{-1} when fitted to a simple exponential decay. More generally we conclude that spin-spin decay mechanisms will be very strong in spin systems at these concentrations unless simultaneously (i) the spin system has a large inhomogeneous broadening to suppress the direct spin-flip effect

and (ii) the optical transition has a magnetic moment change $\Delta(g_m)$ which is very small and therefore suppresses the frequency-diffusion mechanism.

Finally, we have concluded that the direct spin-flip process is inhibited for ions in the long-wavelength tail of the sample absorption line, since a slower photon-echo decay is observed with the laser tuned to this part of the line. This behavior was explained in terms of the presence of the optical spectra of weakly exchange-coupled Cr ions, or long-range pairs, in the tail of the inhomogeneously broadened single-ion R_1 line.

ACKNOWLEDGMENTS

It is a pleasure to acknowledge the constant support and encouragement of Professor I. D. Abella throughout all phases of this research. I am indebted also to L. Q. Lambert for many helpful comments and invaluable assistance in performing the experiments, and to C. Y. Pang and S. Paranjape for assistance in the laboratory and in numerical analysis. The general finanical support of the Army Research Office (Durham) in the initial phases of this work is gratefully acknowledged.

APPENDIX

In this Appendix we wish to motivate and make estimates of the quantities σ_i^2 and γ of Eq. (37) in terms of the spin flip-flop dynamics and compare the estimates with those which hold when spin-lattice relaxation dominates. Writing the local field B_i as the sum of contributions from the neighboring spins, we obtain

$$\langle B_i(T+t'')B_i(T+t')\rangle_T = \sum_{j,k} \langle B_{ij}(T+t'')B_{ik}(T+t')\rangle_T \ . \tag{A1}$$

For spin-spin flip flops the only terms which are not uncorrelated are

$$\sum_{j<k} (\langle B_{ij}B_{ij}\rangle + \langle B_{ij}B_{ik}\rangle + \langle B_{ik}B_{ij}\rangle + \langle B_{ik}B_{ik}\rangle) \ , \tag{A2}$$

where we have dropped the arguments of the B's for the moment, and where ions j and k undergo the flip flop. But in this case $\mu_j^z\mu_k^z$ is constant so that

$$\langle \mu_j(T+t'')\mu_k(T+t')\rangle_T = -\langle \mu_j(T+t'')\mu_j(T+t')\rangle_T , \tag{A3}$$

where the z superscripts are understood. Thus we obtain

$$\langle B_i(T+t'')B_i(T+t')\rangle_T = \sum_{j<k} \langle \mu_j(T+t'')\mu_j(T+t')\rangle_T \times \left(\frac{1-3\cos^2\theta_{ij}}{r_{ij}^3} - \frac{1-3\cos^2\theta_{ik}}{r_{ik}^3}\right)^2 \ . \tag{A4}$$

When spin-lattice relaxation dominates, the corresponding expression is

$$\langle B_i(T+t'')B_i(T+t')\rangle_T = \sum_j \langle \mu_j(T+t'')\mu_j(T+t')\rangle_T (1-\cos^2\theta_{ij})^2/r_{ij}^6 \ . \tag{A5}$$

For the case of spin-spin flips the size of the fluctuations in B_i are reduced because the field change due to the spin flips of spin j is opposite to that of spin k. However, the principal contribution to the fluctuations comes from the near neighbors of ion i in which case the difference in the field change, due to spins j and k, is not much less than that due to one spin alone. For example, if $r_{ik} = 2r_{ij}$, then, because of the $1/r^3$ dependence, $\Delta B_{ij} - \Delta B_{ik} = \frac{7}{8}\Delta B_{ij}$. Thus we have chosen to use the expression (A5) to make an estimate of the spectral-diffusion effects because it is much easier to work with than the double sum, Eq. (A4).

Second, to estimate the correlations of the magnetic moments $\langle \mu_j(T+t'')\mu_j(T+t')\rangle$ of Eq. (A4) we shall assume that they are described by a Markoff process, and thus

$$\langle \mu_j(T+t'')\mu_j(T+t')\rangle_T = \langle \mu_j^2(0)\rangle e^{-\gamma_j|t''-t'|} \ , \tag{A6}$$

where for an $S=\frac{3}{2}$ system $\langle \mu_j^2(0)\rangle = \frac{5}{4}(g\mu_B)^2$. We shall identify γ_j with γ the average spin-spin flip rate in the crystal. This assumption ignores the fact that γ_j varies from one ion j to the next according to the location of its neighboring spins. This contrasts again with the situation for spin-lattice relaxation where γ may be identified with the spin-lattice relaxation rate T_1^{-1} *independent* of the magnetic environment. We shall relate γ to calculated magnetic resonance linewidth due to dipolar broadening.[26] The contribution from the off-diagonal, flip-flop matrix elements to the square root of the second moment of the resonance line is approximately one-third of the total. We shall assume that the same ratio applied to the actual linewidth and, therefore, take[26]

$$\gamma = \tfrac{1}{3}\Delta\omega_{\mathrm{FWHM}} = \tfrac{1}{3}(7.6n/\hbar)(g\mu_B)^2 = 2\times 10^{10} f \ \mathrm{sec}^{-1} \ . \tag{A7}$$

The considerations of this Appendix have been presented in very qualitative fashion but the estimates should be sufficient at least to set an upper limit for the magnitude of the spectral-diffusion decay in ruby.

*Supported in part by the National Science Foundation, under Grant No. GP-18622, and in part by Advanced Research Projects Agency, under Contract No. DAHC 15-67-C-0220.

†Presented as a thesis to the Department of Physics, The University of Chicago, in partial fulfillment of the requirements for the Ph. D. degree.

‡National Science Foundation Predoctoral Trainee.

§Present address: Department of Physics, New York University, New York, N. Y. 10003.

[1]I. D. Abella, N. A. Kurnit, and S. R. Hartmann, Phys. Rev. 141, 391 (1966).

[2]N. A. Kurnit, I. D. Abella, and S. R. Hartmann, in *Physics of Quantum Electronics*, edited by P. L. Kelley *et al.* (McGraw-Hill, New York, 1966), p. 267.

[3]C. K. N. Patel and R. E. Slusher, Phys. Rev. Letters 20, 1087 (1968).

[4]I. D. Abella and H. Z. Cummins, J. Appl. Phys. 32, 1177 (1961).

[5]B. Bölger and J. C. Diels, Phys. Letters 28A, 401 (1968).

[6]G. F. Imbusch, Phys. Rev. 153, 326 (1967); R. C. Powell, B. DiBartolo, B. Birang, and C. S. Naiman, *ibid.* 155, 296 (1967); R. J. Birgeneau, J. Chem. Phys. 50, 4282 (1969); S. K. Lyo, Phys. Rev. B 3, 3331 (1971).

[7]A. L. Schawlow, D. L. Wood, and A. M. Clogston, Phys. Rev. Letters 3, 271 (1959); A. L. Schawlow and L. F. Mollenauer, Phys. Rev. 168, 309 (1968); P. Kisliuk and W. F. Krupke, J. Appl. Phys. 36, 1025 (1965); M. J. Berggren, thesis (Stanford University, 1969) (unpublished); M. J. Berggren, G. F. Imbusch, P. L. Scott, Phys. Rev. 188, 675 (1969).

[8]H. Statz, L. Rimai, M. J. Weber, G. A. deMars, and G. F. Koster, J. Appl. Phys. 32, 218S (1961); F. J. Milford, M. Kreitman, and J. G. Daunt, in *Proceedings of the Eighth International Conference on Low Temperature Physics* (Butterworth's, London, 1963).

[9]Recently, however, a "laser-induced line-narrowing" technique was used to measure an optical linewidth in ruby smaller than the inhomogeneous width of about 0.1 cm^{-1}. [A. Szabo, Phys. Rev. Letters 25, 924 (1970); 27, 323 (1971).] We comment on this measurement further in Sec. IV.

[10]D. E. McCumber and M. D. Sturge, J. Appl. Phys. 34, 1682 (1963); Y. Tanabe, Progr. Theoret. Phys. (Kyoto) Suppl. 14, 17 (1960).

[11]L. Q. Lambert, A. Compaan, and I. D. Abella, Phys. Letters 30A, 153 (1969).

[12]D. Grischkowsky and S. R. Hartmann, Phys. Rev. B 2, 60 (1970).

[13]L. G. Rowan, E. L. Hahn, and W. B. Mims, Phys. Rev. 137, A61 (1965); D. Grischkowsky and S. R. Hartmann, Phys. Rev. Letters 20, 41 (1968).

[14]A. Compaan, L. Q. Lambert, and I. D. Abella, Phys. Rev. Letters 20, 1089 (1968).

[15]S. Sugano and Y. Tanabe, J. Phys. Soc. Japan 13, 880 (1958).

[16]The optical linewidth increases from 0.1 cm^{-1} for low concentrations to 1 cm^{-1} at 1% Cr. See R. C. Powell, B. DiBartolo, B. Birang, and C. S. Naiman, J. Appl. Phys. 37, 4973 (1966). Thus the laser linewidth of about 0.02 cm^{-1} is considerably narrower than the sample absorption line for all cases, and for circularly polarized pulses, ions from only one of the four equally populated ground states are excited so that, at most, approximately 5% of the Cr ions "see" the pulses. See also D. F. Nelson and M. D. Sturge, Phys. Rev. 137, A1117 (1965).

[17]A. Compaan, L. Q. Lambert, and I. D. Abella, Opt. Commun. 3, 236 (1971); L. Q. Lambert, A. Compaan, and I. D. Abella, Phys. Rev. A 4, 2022 (1971).

[18]W. B. Mims, K. Nassau, and J. D. McGee, Phys. Rev. 123, 2059 (1961).

[19]J. R. Klauder and P. W. Anderson, Phys. Rev. 125, 912 (1962).

[20]W. B. Mims, Phys. Rev. 168, 370 (1968).

[21]U. Fano, Rev. Mod. Phys. 29, 74 (1957).

[22]R. H. Dicke, Phys. Rev. 93, 99 (1954).

[23]F. A. Hopf and M. O. Scully, Phys. Rev. 179, 399 (1969).

[24]J. C. Gill, Proc. Phys. Soc. (London) 79, 58 (1962).

[25]P. W. Anderson, Phys. Rev. 82, 342 (1951).

[26]A. Abragam, *The Principals of Nuclear Magnetism* (Oxford U. P., New York, 1961), p. 126.

[27]A. A. Manenkov and V. B. Federov, Zh. Eksperim. i Teor. Fiz. 38, 1042 (1960) [Sov. Phys. JETP 11, 751 (1960)]; W. J. C. Grant and M. W. P. Strandberg, Phys. Rev. 135, A727 (1964).

[28]C. Kittel and Elihu Abrahams, Phys. Rev. 90, 238 (1953); J. H. Van Vleck, *ibid.* 74, 1168 (1948).

[29]B. Herzog and E. L. Hahn, Phys. Rev. 103, 148 (1956); P. W. Anderson, J. Phys. Soc. Japan 9, 316 (1954).

[30]See, for example, R. Kubo, *Statistical Mechanics* (North-Holland, Amsterdam, 1965), p. 87.

[31]For a discussion of Markoff processes see, e.g., M. C. Wang and G. E. Uhlenbeck, Rev. Mod. Phys. 17, 323 (1945), reprinted in *Selected Papers on Noise and Stochastic Processes*, edited by Nelson Wax (Dover, New York, 1954).

[32]L. Q. Lambert (unpublished).

[33]C. P. Slichter, *Principles of Magnetic Resonance* (Harper and Row, New York, 1963), p. 58.

[34]A. J. DeMaria, D. A. Stetser, and H. Heynau, Appl. Phys. Letters 8, 174 (1966).

[35]*Note added in proof.* The effects of optical energy transfer on luminescent decay have been considered recently by Grant [Phys. Rev. B 4, 648 (1971)]. He discusses in detail the method of averaging over "frozen-in" configurations, employed in Secs. III B and III C.